Polyaniline hybridization promotes photo-electro-catalytic removal of organic contaminants over 3D network structure of rGH-PANI/TiO$_2$ hydrogel

Wenquan Cui*, Jing He, Huan Wang, Jinshan Hu, Li Liu, Yinghua Liang*

College of Chemical Engineering, Hebei Key Laboratory for Environment Photocatalytic and Electrocatalytic Materials, North China University of Science and Technology, Tangshan 063210, PR China

ARTICLE INFO

ABSTRACT

Herein, reduced graphene oxide-polyaniline/titanium dioxide composite (rGH-PANI/TiO$_2$) with three-dimensional (3D) network structure was successfully synthesized by a two-step method involving a hybridization process and a water bath approach. The rGH-PANI/TiO$_2$ hydrogels showed excellent performance in the degradation of various organic contaminants. The efficiencies of rGH-PANI/TiO$_2$ hydrogels for photo-electro-catalytic (PEC) removal of phenol was 100% much higher than that of photocatalysis (42%) and electrocatalysis (68%) alone. Meanwhile, the efficiencies of bisphenol A and 2,4-dichlorophenol were 100% after 4.5 and 3.5 h. More important, rGH-PANI/TiO$_2$ hydrogels have excellent mineralization ability for coking wastewater, and the removal rates of total organic carbon (TOC) and chemical oxygen demand (COD) reached 53.1% and 71.9%, respectively. Furthermore, the activities of rGH-PANI/TiO$_2$ for PEC degradation of phenol were also investigated under different conditions, such as phenol concentrations, sodium sulfate (Na$_2$SO$_4$) concentrations, and pH value. The results revealed that rGH-PANI/TiO$_2$ had outstanding PEC performance for the degradation of contaminants. This is because PANI is an excellent material for transporting holes. The large π bonds on graphene promote the rapid transfer of electrons. The addition of PANI and rGH promotes the separation of electron-hole pairs, and the degradation efficiencies of contaminants were improved. Therefore, the reported rGH-PANI/TiO$_2$ composites have excellent potential to purify industrially generated wastewater thanks to their outstanding PEC performance.

1. Introduction

Photo-electro-catalytic (PEC) technology is considered to be an effective approach for suppressing the recombination of electron-hole pairs generated by a semiconductor [1]. The electrons generated on a photo-anode (i.e., a photo-catalyst is fixed on a conductive substrate) are driven to the cathode by a certain bias voltage that inhibits the electron-hole pairs recombination, improves quantum efficiency, and avoids the problems of recycling powder catalysts. Recently, the PEC method has been widely applied for the decomposition of water (H$_2$O) to hydrogen [2–5], degradation of organic pollutants [6–8], and reduction of carbon dioxide (CO$_2$) [9,10]. For example, zhao et al. [6] prepared a TiO$_2$/Ti photoanode and its application as the active material for decomplexation of Cu-EDTA and recovery of Cu^{2+} ions in the PEC process. It may provide a promising alter for destruction of metal complex and recovery of metal ions.

Thin film electrodes are currently employed as the photoelectrodes

for photo-electro-catalysis [11–15]. Zhu et al. [16] reported that a TiO$_2$/g-C$_3$N$_4$ (TCN) thin film electrodes completely degraded phenol via the TCN-0.3 with 1.5 V bias after 1.5 h under simulated solar irradiation with a 100% TOC removal rate; 45% of the TOC for the coking wastewater was removed after 5 h. Wang et al. [17] also reported (RGO)/TiO$_2$ thin film electrode that offered high photocatalytic efficiencies for degradation of RhB and acid orange II. However, research on PEC degradation is used only with single organic contaminants due to the small contact area between the catalysts and the contaminants on the thin film electrode. This results in fewer active sites and weaker adsorption capacity [18]. The activities of the catalysts for PEC degradation of mixed wastewater also have been explored only to a limited degree. Therefore, looking for PEC materials with a larger specific surface area, more active sites, better catalytic ability, and degradation of mixed contaminants is an urgent task in the large-scale application of photo-electro-catalysis.

Graphene has a two-dimensional honeycomb structure with planar

---

* Corresponding authors.
E-mail addresses: wqcui@ncst.edu.cn, wkcui@163.com (W. Cui), liangyh@ncst.edu.cn (Y. Liang).

properties of nonporous surface adsorption and π-π adsorption [19]. The planar conjugated π bond of graphene can rapidly capture and transport electrons to effectively separate the electrons and holes [20]. Unlike two-dimensional graphene, three-dimensional (3D) graphene hydrogels with a macroscopic network structure show a larger specific surface area, more developed pore structures, and higher surface adsorption ability [21–23].

We recently proposed a series of photocatalytic systems based on the composites of graphene hydrogel. The photocatalytic degradation ability of the systems has been efficiently improved by the synergism of graphene and TiO_2. A 3D graphene hydrogel system (80% TiO_2-rGH) showed excellent adsorption ability with a capacity of about 476.2 mg/g in the process of degradation of bisphenol A (BPA) [24]. Another 3D TiO_2-rGH system also exhibited superb adsorption-photocatalysis performance removing 100% Cr(VI) from a solution containing (5 mg/L) within 30 min under ultraviolet (UV) irradiation. Under continuous flow conditions, the adsorption-photo-catalytic activity of TiO_2-rGH could be nicely maintained, and the Cr(VI) removal percentage remained at 100% for a prolonged period [25]. Although, the 3D TiO_2-rGH hydrogel electrode reported by Zhang [24] could completely degrade BPA (20 mg/L) in 5 h through the synergistic effect of adsorption and photo-electro-catalysis, the composites of graphene and TiO_2 can only be excited by 3%~5% UV light in the sun. The poor use of visible light, low quantum yield, and the easier recombination of electrons and holes limits its application in catalysis.

In recent years, conductive polyaniline (PANI) has attracted tremendous attention owing to the advantages of its simple preparation, good stability, low cost, and effective charge transfer [26]. For instance, the visible light photocatalytic performance of TiO_2 was significantly enhanced by modifying PANI [27]. Pandiselvi et al. [28] prepared a novel ternary heterostructure of carbon nitride/polyaniline/ZnO (CN-NS/PANI/ZnO). The coupling synergistic effect of PANI and ZnO and the sensitization of PANI enhanced the absorption of visible light of CN. At the same time, the degradation efficiencies of CN-NS/PANI/ZnO were 2.6 and 2.3 times higher than CN toward Methylene blue (MB) and 4-chlorophenol (4-CP) degradation under visible light irradiation.

Neelgund et al. [29] prepared PANI and graphene nanocomposites (GR-PANI), which accelerated the separation of charge carriers generated during photolysis. These expanded the absorption range of sunlight and promoted photocatalytic activity. The PANI–GR–TiO_2 hybrid designed by Jing et al. [30] displayed promising oxygen evolution reaction (OER) activity for PEC water oxidation due to the addition of PANI. This can extend the range of sunlight absorption and increase the rapid separation of charge carriers generated during photocatalysis. Meanwhile, Jiang et al. [31] prepared a 3D hydrogel system constructed from polyaniline/carbon nitride (PANI/CNNS) via the *in situ* polymerization. It is excellent at removing organic contaminants for PANI/CNNS composite hydrogels.

In this paper, a ternary nanocomposite of rGH-PANI/TiO_2 electrode with 3D interconnection network was constructed via a hybridization process and a water bath approach. The as-prepared ternary rGH-PANI/TiO_2 showed remarkable PEC activity and photostability for UV light degradation of pollutants. The enhanced performance was facilitated by the introduction of PANI that significantly broadened the absorbance range of TiO_2. In addition, the quinone ring on PANI interacted with the π-π bond on graphene creating a large π bond, which enhanced the rapid charge transfer between PANI and graphene. The rGH-PANI/TiO_2 with 3D network structure possess large surface areas, plenty of mesopores with open pore frameworks, so that much more nano-particles could be immobilized in the inside and on the surface of the rGH hydrogel. The large surface areas can provide more catalytic activity sites, which can promote that the phenol molecules were adsorbed on the photoelectrode surface for rapid in situ degradation.

The rGH-PANI/TiO_2 hydrogel demonstrated excellent performance for the degradation of refractory phenols, such as phenol, BPA, and 2,4-dichlorophenol. Moreover, the modified rGH-PANI/TiO_2 electrode was successfully applied to degrade coking wastewater. It degraded organic contaminants in practical samples. The influence of the PANI and rGH content in the nanocomposites on the degradation of phenol was also investigated and optimized to achieve a high-performance material. Furthermore, the morphology, optical properties, and catalytic activity of the composites were investigated in detail.

2. Experimental

2.1. Preparation of samples

PANI was obtained from Shanghai Xin Yue Fine Chemical Co., Ltd. TiO_2 (P25 with 80% of anatase and 20% of rutile) was purchased from Evonik Degussa Company. Graphene oxide was purchased from TIMES-NANO (Chengdu, Sichuan, China). All reagents were of analytical grade and were used without further purification. The water employed in the experiments was deionized water.

The PANI/TiO_2 nanocomposites were prepared as follows: PANI was added into a clean beaker with 200 mL deionized water followed with ultra-sonication until the PANI was evenly dispersed. The same amount of TiO_2 was added to the PANI slurry and was under sonication for 12 h until uniform. The solution was allowed to stand. The resulting precipitate was filtered and washed three times with deionized water. The products were dried in an oven at 80 °C for 24 h, and the dried products were finally ground in an agate mortar to obtain pale blue powder composites catalyst. We obtained PANI/TiO_2 hybrid photo-catalysts with a mass ratio of 2.0 Wt.%, 4.0 Wt.%, 6.0 Wt.%, 8.0 Wt.%, and 10.0 Wt.%. (The ratio is the mass percentage of PANI at PANI/TiO_2.)

The preparation of 3D network rGH-PANI/TiO_2 hydrogel is shown in Scheme 1. The prepared graphene oxide (GO) solution was sonicated for 1 h to evenly disperse the material. Five drops of polyethylene glycol 200 was added to the mixture of PANI/TiO_2 with grinding for 5 min followed by adding a certain amount of GO solution into the mixture of PANI/TiO_2 with continued grinding for 2 min until the slurry was homogeneous. The ternary mixture was sonicated for 1 h to form an uniform slurry. A certain amount (10-fold amount of GO) of ascorbic acid (VC) was added and ultra-sonication continued for an additional 30 min. Subsequently, 1 mL mixed slurry was added to a 4 × 4.5 × 0.6 cm Teflon mold followed by a 2 × 2.5 cm titanium mesh (80 mesh, pore size 178 μm) placed into the mold. The mold was covered with glass and placed in a constant temperature water bath at 95 °C for 1 h. Finally, ternary composite photoelectrodes with different mass ratios are obtained. The results are recorded as 10% rGH-PANI/TiO_2, 20% rGH-PANI/TiO_2, 50% rGH-PANI/TiO_2, and 80% rGH-PANI/TiO_2, respectively. (The ratio is the mass percentage of GO at rGH-PANI/TiO_2.)

TiO_2 and PANI/TiO_2 thin film electrodes were prepared as follows: a 2 × 2.5 cm photoelectrode of 2.0 mg/cm^2 was prepared by drop-coating on conducting indium tin oxide (ITO) (4 × 2 cm) glass. ITO glass was cleaned three times before preparing the thin film electrodes. The 10 mg of TiO_2 or PANI/TiO_2 were placed in absolute ethanol with polyethylene glycol 2000 and stirred evenly. The TiO_2 and PANI/TiO_2 thin film electrodes were dropped onto ITO conductive glass by glass rods. Finally, After air drying, the as-prepared photoelectrodes were calcined for 30 min at 150 °C to obtain the TiO_2 and PANI/TiO_2 hybrids photoelectrodes.

2.2. Characterization

The microtopography of the materials was as recorded by a Hitachi (Tokyo, Japan) S-4800 field emission scanning electron microscopy (SEM). The morphology and size of the samples were analyzed by an Hitachi HT-7700 with an accelerating voltage of 100 kV. The crystal and phase structure of the samples were characterized by X-ray diffractometer (XRD; Rigaku D/MAX-2500PC, scanning range 5°–80°; Tokyo, Japan) with Cu Kα1 radiation at 40 kV and 100 mA. The
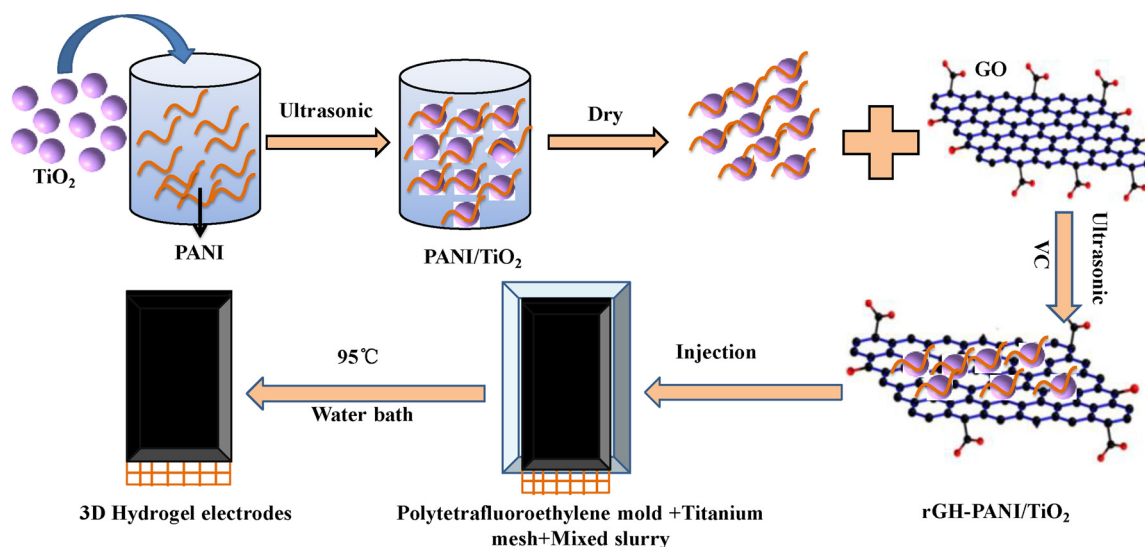
Scheme 1. Preparation of rGH-PANI/TiO$_2$ hydrogel electrode with 3D network structure.

structure of the sample was analyzed by Thermo Nicolet™ Avatar 370 spectrometer (Thermo Fisher Scientific, Waltham, MA, USE) Fourier transform infrared spectrometer (FTIR) using KBr as the reference from 4000-400 cm^{-1}.

The atomic structure and electronic properties of the samples were analyzed by microscopic confocal Raman spectroscopy (HORIBA HR800, Irvine, CA, USA) with an excitation wavelength of 524 nm. The chemical states of the samples were analyzed by X-ray photoelectron spectroscopy (XPS; KRATOS XSAM800; Kratos Analytical, Manchester, UK). Ultraviolet-visible diffuse reflectance absorption spectroscopy (UV–vis DRS) was recorded on a Shimadzu (Shimadzu Instruments Co., Ltd., Kyoto, Japan) UV–vis diffuse reflectance spectrometer (UV-2500 with a test wavelength of 200–800 nm), and barium sulfate (BaSO$_4$) was the reference. Photoluminescence spectra (PL) were acquired at room temperature using a Hitachi F-7000FL luminescence spectrophotometer with an excitation wavelength of 270 nm. Brunauer-Emmett-Teller (BET) surface area was conducted on a Micromeritics (Micromeritics Instrument Corporation, Norcross, GA, USA) 3020 instrument under nitrogen (N$_2$) adsorption–desorption.

2.3. Photoelectrochemical properties

Photoelectrochemical measurements were performed on a CHI (Chenhua, Shanghai) 660E electrochemical workstation with a single chamber quartz cell. A 500 W mercury lamp (CEL-M500, total luminous power of 15 W, photoelectric current density of 41 mW/cm^2) purchased from Beijing Zhong Jiao Jin Yuan Technology Co. Ltd was used. This served as the UV light source with a UV cut-off filter (320 nm); 0.5 M sodium sulfate (Na$_2$SO$_4$) was the electrolyte. TiO$_2$, PANI/TiO$_2$, and rGH-PANI/TiO$_2$ hybrid photoelectrodes were the working electrodes, a saturated calomel electrode (SCE) was the reference electrode, and a Platinum (Pt) wire was the counter electrode. A mercury lamp was placed 10 cm in front of the working electrode. Electrochemical impedance spectroscopy (EIS) was performed from 1–10^5 Hz with 5 mV alternating current signal. Current versus potential measurement (LSV) was measured at a scan rate of 50 mV s^{-1}. Photocurrent response was obtained from the potentiostatic measurements (current vs. time I-t) under UV irradiation.

2.4. PEC degradation of organic pollutants

The PEC degradation of origin contaminants are shown in Scheme 2. PEC degradation experiments were performed in a 5 × 5 × 5 cm self-made quartz reactor. A 500 W mercury lamp was used as the UV light
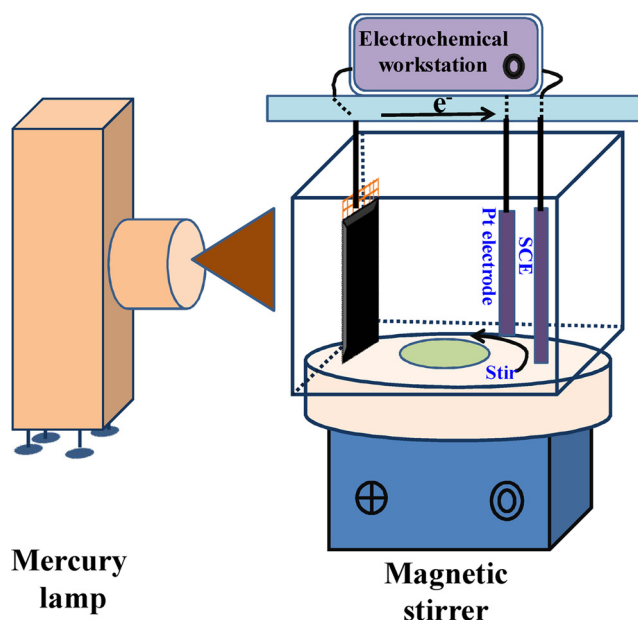
Scheme 2. PEC degradation system.

source with a UV cut-off filter (320 nm). The bias voltage was provided by CHI 660E electrochemical workstation. 150 mg/L Na$_2$SO$_4$ was used as electrolyte and SCE and Pt wire as the reference electrode and counter electrode, respectively. TiO$_2$ and rGH-PANI/TiO$_2$ hybrid photoelectrodes were employed as the working electrodes. The bottom of the working electrode was 2 cm to the bottom of the reactor, and the mercury lamp was placed 10 cm in front of the working electrode. About 1.1 mL solution was taken out every 30 min. The particles were separated by high-speed centrifugation and filtrated with a 0.22 um filter. Phenol concentration was analyzed by high-performance liquid chromatography (HPLC). Total Organic Carbon (TOC, TOC-L CPH) purchased from SHIMADZU Instruments Co., Ltd. was employed to analyze the degree of mineralization of the organics, and the COD value was determined by potassium dichromate oxidation.

To evaluate the stability and recyclability of the catalysts, TiO$_2$ thin film electrode and rGH-PANI/TiO$_2$ hydrogel electrode placed in a self-made quartz reactor were respectively used to degrade 100 mL phenol (10 mg/L) and repeated the process five times. The total reaction time of degradation was 8 h. The final concentration of phenol was
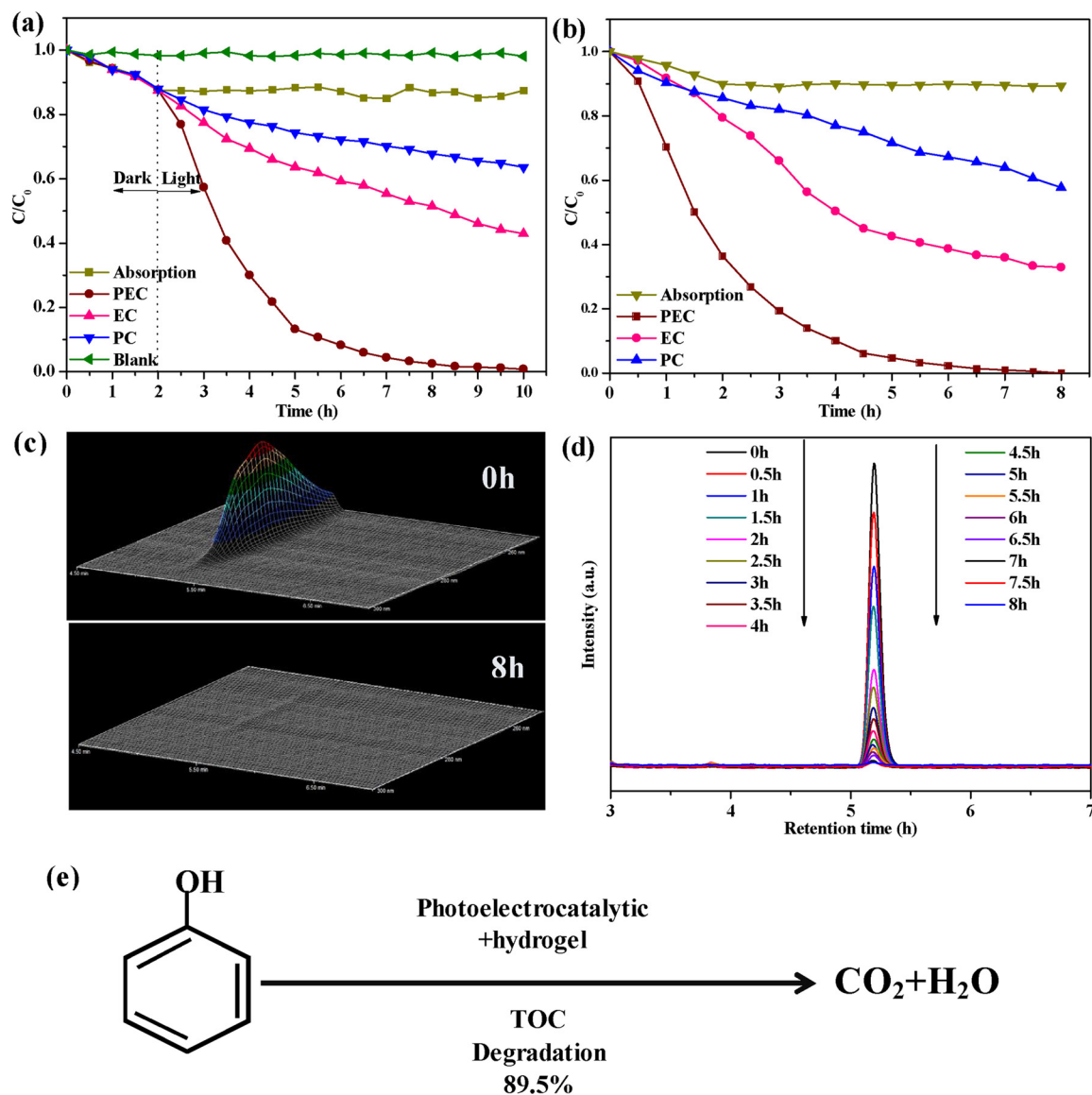
Fig. 1. rGH-PANI/TiO$_2$ PEC degradation of phenol (the concentration of phenol was 10 mg /L, 1.0 V bias, 500 W mercury lamp, λ ≥ 320 nm): (a) activity comparison of adsorption, photocatalysis, electrocatalysis, and photo-electro-catalysis; (b) activity comparison of adsorption, adsorption-photocatalysis, adsorption-electrocatalysis, and adsorption-photo-electro-catalysis; (c) 3D HPLC chromatographic spectra of phenol degradation (0 h and 8 h); (d) HPLC chromatograms of phenol solutions; and (e) schematic diagram of phenol degradation process.

determined by HPLC. After each test, the electrode was washed with deionized water three times for the next PEC degradation test.

In addition to phenol, the same method was used to investigate the PEC degradation of 2,4-dichlorophenol, BPA, mixture wastewater, and coking wastewater.

3. Results and discussion

3.1. Hybridization of PANI accelerates the PEC performance of 3D network rGH-PANI/TiO$_2$ hydrogel

The experiments of rGH-PANI/TiO$_2$ for degradation of phenol under different conditions are shown in Fig. 1. Fig. 1(a) reveals that the system can achieve adsorption equilibrium after 2 h in the dark. The efficiencies of rGH-PANI/TiO$_2$ for degradation of phenol under photocatalytic and electrocatalytic conditions were only 37% and 57% after 10 h, respectively. However, the efficiency could achieve 100% under PEC conditions. This indicated that photo-electro-catalysis can better degrade organic contaminants. The experiment with rGH-PANI/TiO$_2$

for degradation of phenol was conducted without pre-adsorption (as shown in Fig. 1(b)). The degradation efficiency of the system reached 100% after 7 h, which indicated that the use of synergetic photo-electro-catalysis and adsorption approach could more effectively degrade contaminants. In addition, the degradation efficiency of PEC was much higher than photocatalysis (42%) and electrocatalysis(68%) obtained from Fig. 1(b).

Fig. 1(c) shows the 3D HPLC chromatographic spectra of a ternary rGH-PANI/TiO$_2$ complex for degradation of phenol before and after the PEC degradation process. The peaks corresponding to the phenol disappeared—these data agreed with Fig. 1(d). As the reaction proceeded, the corresponding peak area gradually decreased and there were no other peaks in Fig. 1(d). This demonstrated that phenol was degraded to CO$_2$ and H$_2$O in the process of the PEC reaction. The mineralization process of phenol was shown in Fig. 1(e). The removal rate of TOC could reach 89.5% (Fig. 19).

A series of experiments of rGH-PANI/TiO$_2$ for degradation of 2,4-dichlorophenol, BPA, and the mixture of phenol, 2,4-dichlorophenol and BPA were conducted in order to prove that rGH-PANI/TiO$_2$ could
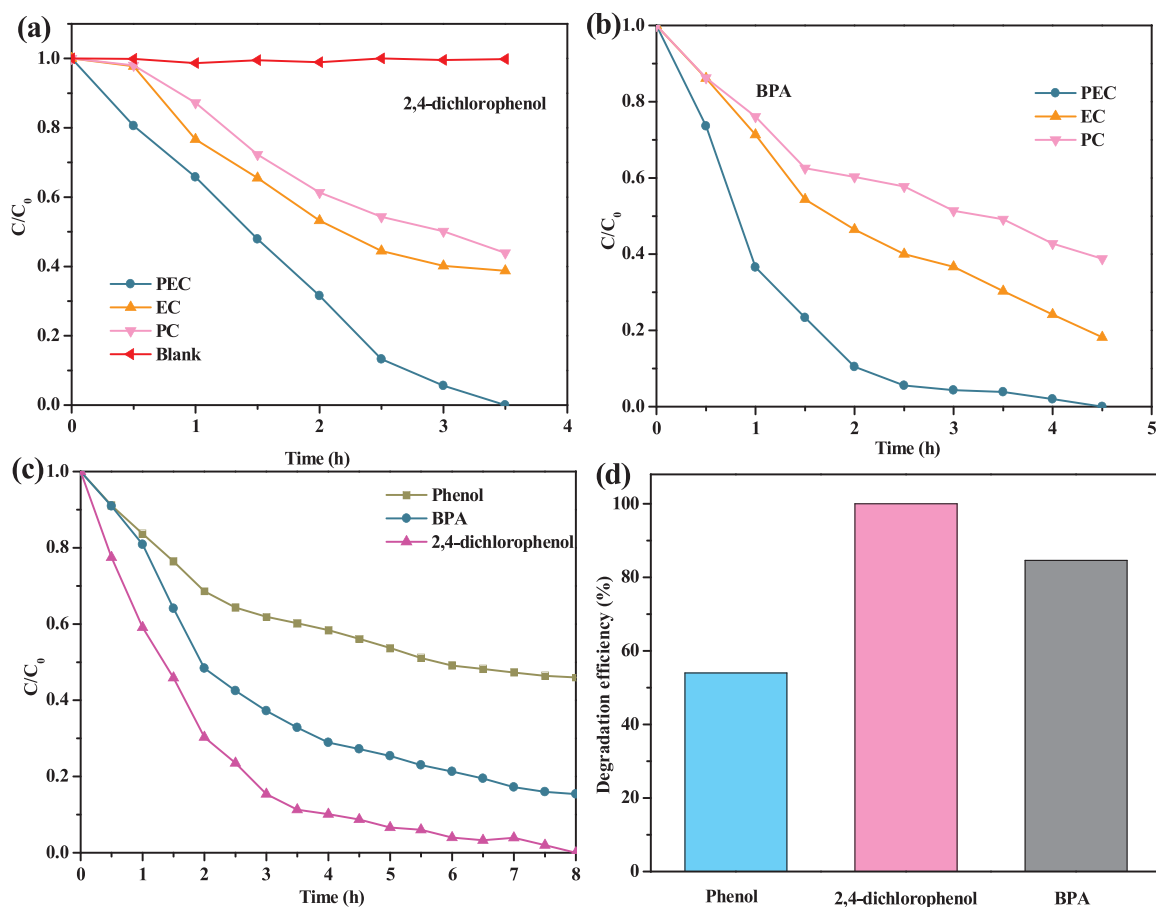
Fig. 2. Degradation of different pollutants of (a) 2,4-dichlorophenol; (b) BPA; and (c) a mixture of phenol, BPA and 2,4-dichlorophenol. (d) Degradation efficiency for a mixture of phenol, BPA, and 2,4-dichlorophenol over rGH-PANI/TiO$_2$ photoelectrode. (The concentration of the mixture was 10 mg/L, 1.0 V bias, 500 W mercury lamp, and $\lambda \geq 320$ nm.).

degrade a variety of organic contaminants and mixed pollutants. The efficiencies of rGH-PANI/TiO$_2$ for PEC, electrocatalytic and photocatalytic degradation of 2,4-dichlorophenol (10 mg/L) could reach 100%, 61.3%, and 56.1% after 3.5 h, respectively (Fig. 2(a)) . The results revealed that the PEC degradation performance of rGH-PANI/TiO$_2$ was much higher than that of electrocatalysis and photocatalysis. Fig. 2(b) reveals that the performance of rGH-PANI/TiO$_2$ for PEC (100%) degradation of BPA was much better than that of electrocatalysis (81.8%) and photocatalysis (61.2%). More significantly, the efficiencies of rGH-PANI/TiO$_2$ for PEC degradation of the mixture, including phenol, 2,4-dichlorophenol, and BPA, could reach 54.3%, 100%, and 85%, respectively (Fig. 2(c), (d)). These results revealed that rGH-PANI/TiO$_2$ could degrade a variety of organic contaminants or mixed pollutants.

SEM, TEM, and real images of rGH, PANI, TiO$_2$, and rGH-PANI/TiO$_2$ are shown in Fig. 3. The left view of Fig. 3(a) illustrates that the rGH-PANI/TiO$_2$ hydrogel electrode has a certain macro-thickness. The macroscopic image of rGH-PANI/TiO$_2$ hydrogel electrode is depicted in Fig. 3(b). The ternary hydrogel electrode is well attached to the titanium mesh, and this provides convenient conditions for the adsorption of organic contaminants. The SEM image of rGH is shown in Fig. 3(c), and it is obvious that rGH has micron-size pores with a 3D network structure. The large pores are mainly due to hydrophobicity, π-π conjugation, and electrostatic repulsion after the graphene oxide was reduced [32,33], which could provide more activity sites for the adsorption of organic contaminants. The TEM of rGH is shown in Fig. 3(d). It is obvious that rGH is a transparent sheet with multiple folds. The PANI structure is prone to accumulate (Fig. 3(e)). Meanwhile, TiO$_2$ with small particle size is also prone to agglomerate (Fig. 3(f)). Graphene and PANI/TiO$_2$ compound can effectively reduce

the agglomeration of PANI and TiO$_2$. The SEM of the ternary complex rGH-PANI/TiO$_2$ revealed that PANI/TiO$_2$ was uniformly distributed in the 3D rGH network (Fig. 3(g)). Although TiO$_2$ was easy to agglomerate, the interacted 3D rGH nicely reduced the agglomeration of TiO$_2$. The TEM image of the ternary complex rGH-PANI/TiO$_2$ illustrated that the lattice fringes of TiO$_2$ were obvious (Fig. 3(h)). The interplanar spacing (d = 0.35 nm) corresponded to the TiO$_2$ (101) crystal plane. PANI hybrids were well modified on the surface of the TiO$_2$ thin films, which demonstrated that the ternary complex rGH-PANI/TiO$_2$ was successfully synthesized.

The XRD patterns of the prepared samples are shown in Fig. 4. The wider diffraction peak found in PANI indicated that the existed PANI was predominately amorphous. The diffraction peak at θ = 25.2° was the characteristic peak of the anatase phase [34]. The intensity of TiO$_2$ did not change with the addition of PANI and rGH, indicating that the lattice structure of TiO$_2$ was stable. The diffraction peaks of TiO$_2$ nicely matched the peaks found in PANI/TiO$_2$, rGH-TiO$_2$, and rGH-PANI/TiO$_2$, indicating that the composites were successfully synthesized [35]. There is no obvious diffraction peak of PANI in PANI/TiO$_2$ and rGH-PANI/TiO$_2$, which should be due to the relatively low amounts of PANI and the strong intensity of TiO$_2$ [36].

The specific surface area and pore structure of the prepared rGH and rGH-PANI/TiO$_2$ were obtained by measuring its ability to absorb and desorb N$_2$ (Fig. 5(a)). N$_2$ adsorption–desorption isotherms of samples can be identified as type IV in the International Union of Pure and Applied Chemistry classification (IUPAC) with a typical mesoporous hysteresis loop [37]. The pore size distribution of rGH and rGH-PANI/TiO$_2$ is depicted in Fig. 5(b), suggesting that most of the apertures were about 4 nm. Upon addition of PANI/TiO$_2$, the specific surface area of rGH-PANI/TiO$_2$ (210.8 m^2/g) becomes larger than rGH (189.6 m^2/g),
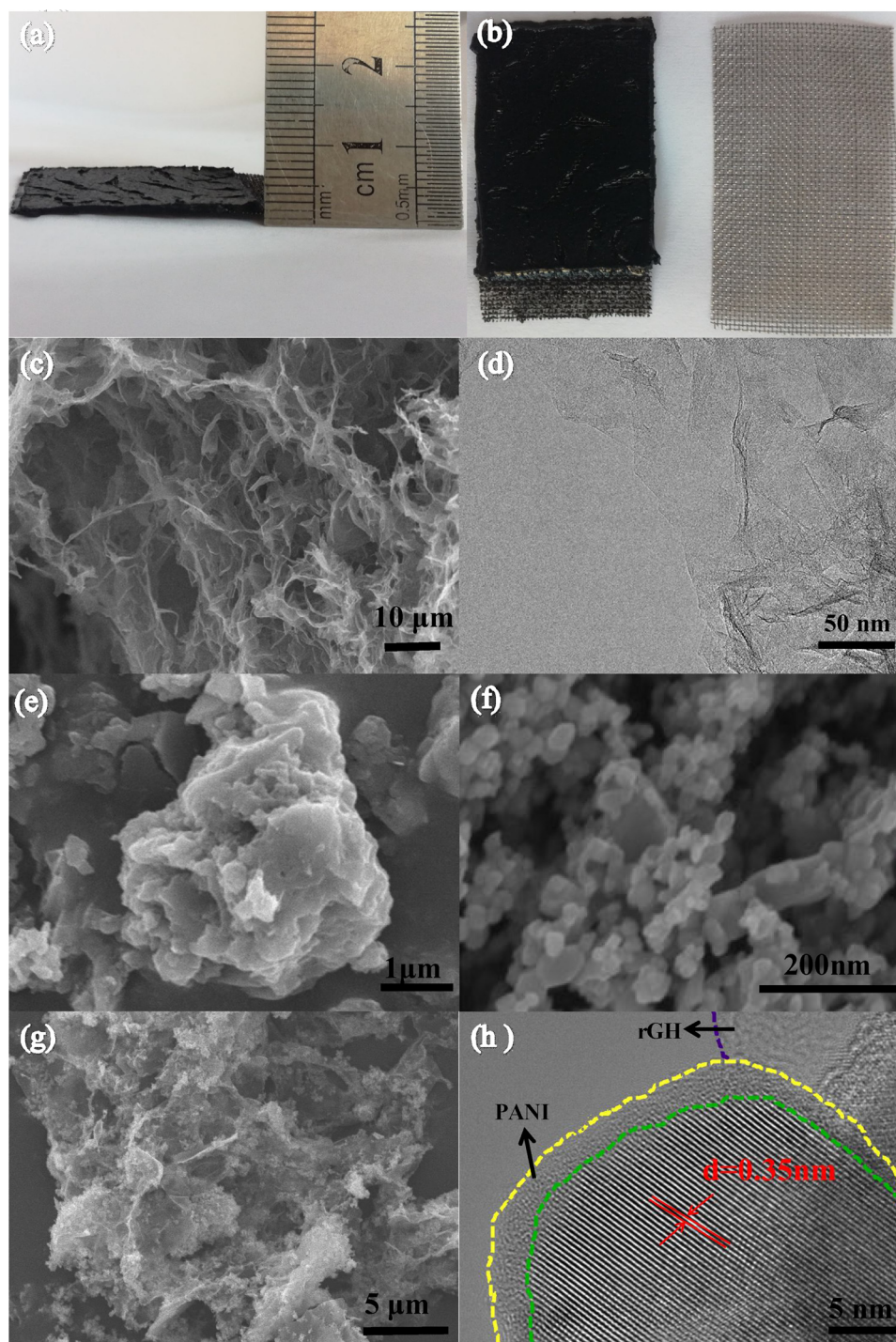
Fig. 3. (a) Left-side view of rGH-PANI/TiO$_2$ hydrogel electrode; (b) rGH-PANI/TiO$_2$ hydrogel electrode and titanium mesh; (c) SEM image of rGH; (d) TEM image of rGH; (e) SEM image of PANI; (f) SEM image of TiO$_2$; (g) SEM image of rGH-PANI/TiO$_2$; and (h) TEM of rGH-PANI/TiO$_2$.

and this is likely because PANI/TiO$_2$ significantly reduced the accumulation of rGH (Table 1). This large specific surface area of the hydrogel electrode can provide more active sites and increase the adsorption capacity.

3.2. Mechanism of PANI hybridization in improving the PEC activity of rGH-PANI/TiO$_2$ hydrogels

The FTIR and Raman spectra of TiO$_2$, PANI, PANI-TiO$_2$, and rGH-PANI/TiO$_2$ are shown in Fig. 6. Fig. 6(a) reveals the chemical interaction between the monomer and composite. The bands at 3400 cm^{-1}

were attributed to the stretching and bending of O−H belonging to adsorbed water (Fig. 6(a)). The peaks at 1587 cm^{-1} were assigned to the C═N stretching vibration of the quinone ring. The peaks at 1474 cm^{-1} were attributed to the C═C stretching vibration peak of the benzene ring. The peaks at 1294 cm^{-1} were due to the C−N peak of PANI [38,39]. The vibrational peak at 1135 cm^{-1} corresponded to the peaks of N═M═N (M stands for quinone ring) [40], which demonstrated a large conjugate bond in rGH-PANI/TiO$_2$ [41]. Meanwhile, the large conjugate bond also facilitated electron transfer. In the rGH-PANI/TiO$_2$, the positions of these peaks shifted to lower wavenumbers, indicating that the intensity of C═C, C−N, and C═N was weak and the
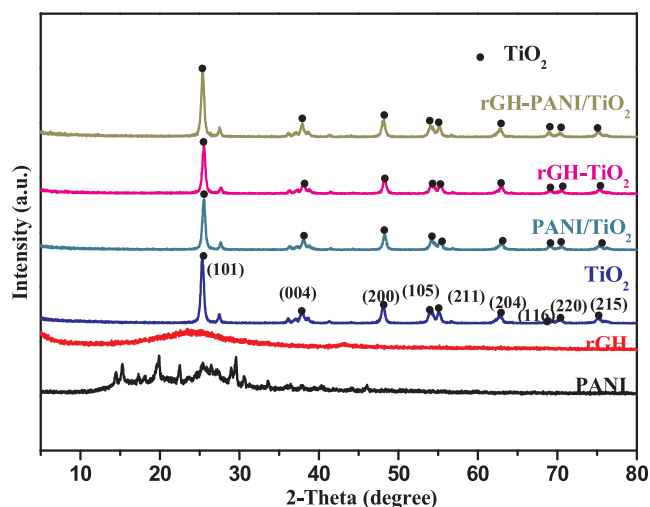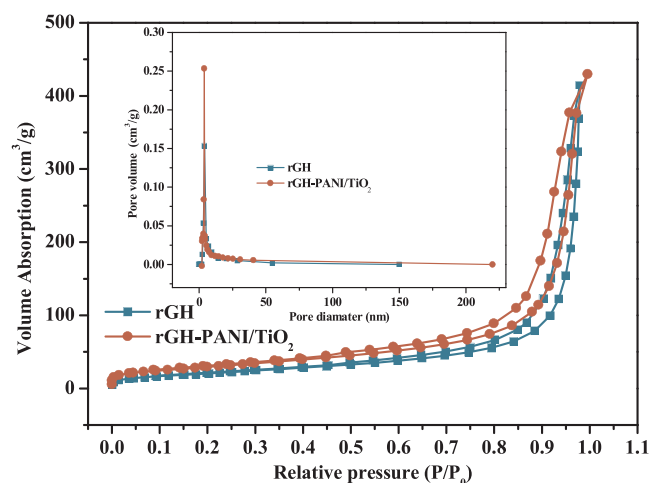
Fig. 4. XRD spectra of the prepared samples.

Fig. 5. (a) N$_2$ adsorption–desorption isotherms and (b) pore size distribution plots of rGH and rGH-PANI/TiO$_2$.

Table 1
Adsorption kinetics parameters of rGH and 20% rGH-PANI/TiO$_2$.

Sample	S$_{BET}$ (m^2/g)	Pore volume (cm^3/g)	Pore diameter (nm)
rGH	189.6	1.7	4.1
rGH-PANI/TiO$_2$	210.8	1.6	3.9

conjugation bond of PANI was stretched. Furthermore, the chemical bonds were formed between rGH and PANI-TiO$_2$. The broad peaks below 1000 cm^{-1} mainly were due to the vibration of Ti−O−Ti [39].

The Raman spectra for different samples are shown in Fig. 6(b). The characteristic peaks of PANI and TiO$_2$ appeared in PANI-TiO$_2$, which indicated that PANI and TiO$_2$ were successfully recombined. The characteristic peaks of TiO$_2$ also were found in the Raman spectra of rGH-PANI/TiO$_2$. The peak of PANI was not found, however, as a result of the relatively low content of PANI.

XPS of the prepared samples is shown in Fig. 7. XPS is used to further study the interaction in the composites. Fig. 7 (a) shows that O, Ti, C, and N were found in the survey scan XPS spectrum. They are associated with O1s, Ti2P, C1s, and N1s. Fig. 7(b) shows that the C1s spectra of rGH-PANI/TiO$_2$ were divided into four peaks at 284.8 eV, 285.4 eV, 286.9 eV, and 288.7 eV, corresponding to carbon atoms in C−C, C−N, C−O, and C═CO, respectively. The C−N peak mainly resulted from the interactions between PANI and rGH, which accelerated

the electron transfer [42]. The peaks at 286.9 eV and 288.7 eV were assigned to the C−O and C═CO functional groups in rGH. The peaks of C−O and C═CO were weaker and mainly were due to the oxygen-containing functional groups (−COOH, −OH). These were reduced after the addition of VC [39,43]. The O1s peak in the prepared samples is shown in Fig. 7(c). In comparison with the TiO$_2$ peak, the peaks of PANI/TiO$_2$, rGH-TiO$_2$, and rGH-PANI/TiO$_2$ shifted, demonstrating that TiO$_2$ interacted with PANI and rGH. The Ti2P spectra of the samples are shown in Fig. 7(d).

The Ti2P spectra were divided into two types: Ti2P$_{3/2}$ and Ti2P$_{1/2}$ [44]. Both of the Ti2p peaks for the composites shifted relative to those for pure TiO$_2$, suggesting that the components interacted. The C1s of rGH and rGH-PANI/TiO$_2$ is illustrated in Fig. 7(e). The peak at 286.1 eV should be assigned to C−O−Ti, revealing that rGH-PANI/TiO$_2$ was successfully synthesized [45]. A shift appearing in the samples indicated that TiO$_2$, PANI, and rGH had chemically interacted with each other.

Fig. 8(a) shows the UV–vis diffuse reflectance spectra of the as-prepared samples. In comparison with TiO$_2$, the absorption edge of PANI/TiO$_2$ and rGH-PANI/TiO$_2$ exhibited different degrees of red shifting. This phenomenon suggests that PANI essentially extended the absorption of TiO$_2$ to the visible-light region. Therefore, PANI improved the catalytic performance of TiO$_2$. The electron recombination efficiency can be measured by photoluminescence spectra [46–48] (Fig. 8(b)). The fluorescence intensities of PANI/TiO$_2$ and rGH-PANI/TiO$_2$ were significantly lower than TiO$_2$, indicating that hybridization between TiO$_2$ and PANI was formed and facilitated the transfer of h$^+$ from the valence band of TiO$_2$ (Eg = −0.2 eV) to the valence band of PANI. Therefore, the interaction promoted the separation of photo-generated charges, which suppressed the recombination of charges and improved the PEC efficiency.

In order to test the influence of PANI on the photoelectric properties of TiO$_2$, a series of photoelectric properties of rGH-PANI/TiO$_2$ were tested. The charge transfer rate is an important indicator to evaluate the photoelectric properties of the composite photoelectrodes; thus, we investigated the photocurrent, impedance, and LSV of TiO$_2$, PANI/TiO$_2$, and rGH-PANI/TiO$_2$ in detail.

The transient photocurrent responses of TiO$_2$, PANI/TiO$_2$, and rGH-PANI/TiO$_2$ are illustrated in Fig. 9(a). This obviously showed that turning on and off the light resulted in changes to the photocurrent response. TiO$_2$, PANI/TiO$_2$, and rGH-PANI/TiO$_2$ could be excited to generate the photocurrent responses at 1.0 V under UV light. Fig. 9(a) revealed that the photocurrent of rGH-PANI/TiO$_2$ obviously increased, and its photocurrent density was about 3.56- and 1.52-fold that of TiO$_2$ and PANI/TiO$_2$, respectively. The enhanced photocurrents could be ascribed to the hybridization between PANI and TiO$_2$ and the high separation efficiency between photo-generated electrons and holes.

Nyquist plots of the photoelectrodes are shown in Fig. 9(b). The semicircular Nyquist plots indicated that the electron transfer at the interface of the electrodes played a prominent role in the electrode process. The impedance of rGH-PANI/TiO$_2$ was much smaller than that of pure TiO$_2$, which proved that the ternary rGH-PANI/TiO$_2$ promoted the rapid separation between electrons and holes.

The PEC properties of TiO$_2$ and rGH-PANI/TiO$_2$ were further studied by LSV (Fig. 9(c)). The photocurrent densities of rGH-PANI/TiO$_2$ and TiO$_2$ were 3.21 mA/cm^2 and 0.94 mA/cm^2 at 2.0 V under UV light, respectively. More significantly, the photocurrent of the ternary composite was 3.41 times that of pure TiO$_2$. The increased photocurrent density of rGH-PANI/TiO$_2$ mainly resulted from the collection and transfer of the electrons on the surface of graphene, which effectively inhibited electron-hole pairs recombination [49]. Fig. 9(d) shows that the characteristic frequency of the rGH-PANI/TiO$_2$ electrode shifted from 350.12 Hz to 753.89 Hz in comparison with pure TiO$_2$. The peak shifts revealed a more rapid electron transport process because the frequency (f) was closely related to the lifetime (τ) of the injected electrons:

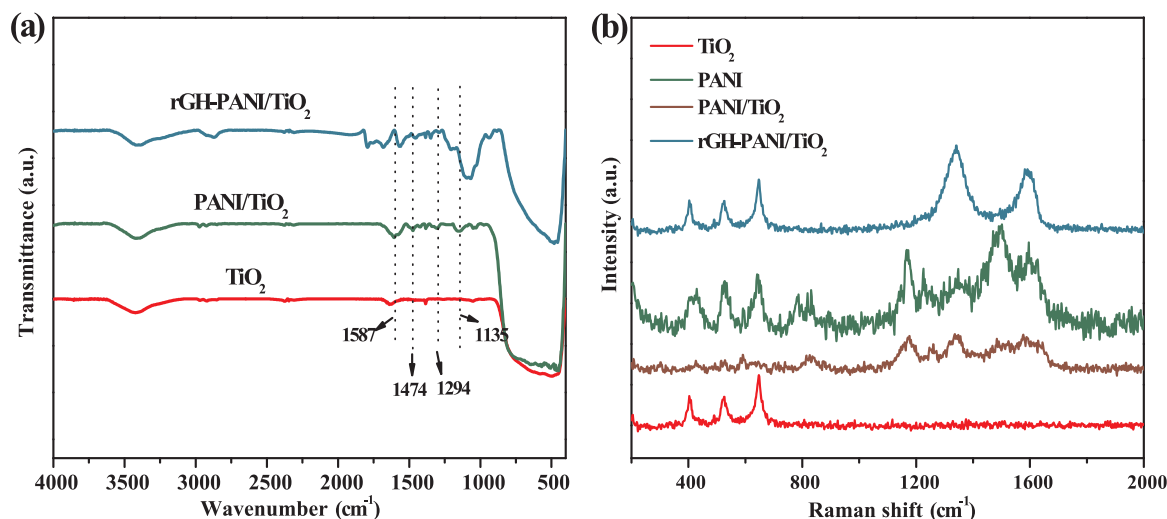**Fig. 6.** TiO_2, PANI, PANI/TiO_2, and rGH-PANI/TiO_2; (a) FTIR spectra; and (b) Raman spectra.

$$\tau \approx 1/ (2\pi f). \quad (1)$$

The calculated electron lifetime (4.55 ms) of rGH-PANI/TiO_2 was 1.16 times higher than TiO_2 (2.11 ms). Conversely, the injected electron lifetime clearly significantly increased to effectively inhibit electron-hole pairs recombination due to the interaction among rGH, PANI, and TiO_2 (Fig. 9(d)).

Next, the PEC experiments of rGH-TiO_2 and rGH-PANI/TiO_2 for the degradation of phenol at various wavelengths were conducted to demonstrate that PANI increased the absorption range of light for TiO_2. Fig. 10(a) shows that the degradation efficiencies of rGH-PANI/TiO_2 increased remarkably in comparison with the rGH-TiO_2 at 400 nm and 420 nm, respectively, which is also consistent with the result of UV–vis diffuse reflection. Additionally, the activities of rGH-PANI/TiO_2 for degradation of phenol were also performed with cut-off filters of $\lambda < 320$ nm, 400 nm, and 420 nm, respectively (Fig. 10(b)). The results revealed that the degradation efficiency of rGH-PANI/TiO_2 could achieve 15% with a cut-off filter of $\lambda < 420$ nm. Therefore, PANI not only effectively separated photo-generated electron-hole pairs but also broadened the absorption range and intensity of TiO_2.

The active species during the PEC process were studied by introducing different trapping agents before the suspension was exposed to UV light. Isopropanol (0.13 ml), EDTA-2Na (0.186 g), and p-benzoquinone (0.054 g) were added into the experiment to capture $\cdot OH$, h^+ and $\cdot O_2^-$, respectively. The PEC performance of rGH-PANI/TiO_2 for the degradation of phenol remained unaffected by isopropanol, indicating that $\cdot OH$ was not the main active species (Fig. 11(a)). When EDTA-2Na and p-benzoquinone were added, however, the degradation efficiencies markedly decreased, suggesting that h^+ and $\cdot O_2^-$ were the main active species in the PEC experiments. The histogram of rGH-PANI/TiO_2 degradation efficiencies is shown in Fig. 11(b).

The PEC mechanism of the ternary rGH-PANI/TiO_2 for degradation of contaminants is deduced as follows (Fig. 12). Both TiO_2 and PANI absorbed the photons when rGH-PANI/TiO_2 composites were illuminated under UV light—they were excited to generate electron-hole pairs. The highest occupied molecular orbital (HOMO) of PANI was located between the conduction band (CB) and valence band (VB) of TiO_2 [31,50,51]. Because the VB of TiO_2 is more positive than the HOMO of PANI, the photo-generated h^+ of TiO_2 could be injected directly into the HOMO of PANI through the well-defined interface. Meanwhile, some researchers also proposed a band position matching which also effectively improve the catalytic activity [52–54]. PANI is an excellent material for transporting holes, and the holes were transferred easily to the surface of the catalysis and oxidized the adsorbed

contaminants directly. Meanwhile, the electrons of PANI transferred to the CB of TiO_2. PANI can induce the flat band potential shift of the hybrids which increases the inner electric field intensity that drives electrons migration from the composites to the coupled metal [55]. They then reached the surface of rGH through hydrogen bonding between TiO_2 and rGH. The photo-generated electrons transferred freely through the titanium mesh basement of the rGH-PANI/TiO_2 electrode to the cathode via the external circuit. The electrons in the cathode reacted with oxygen molecules to generate $\cdot O_2^-$ radicals [56]. These $\cdot O_2^-$ oxidize organic contaminants and eventually phenols were oxidized to small molecules of CO_2 and H_2O [57]. As a result, the charge transfer efficiently inhibited the recombination of photo-generated electron-hole pairs, thereby enhancing the PEC activity of rGH-PANI/TiO_2.

3.3. Optimization of parameters of PEC degradation of organic contaminants and degradation of coking wastewater

Phenol was chose as the model contaminant to evaluate the photocatalytic activity of PANI/TiO_2 upon exposure to UV light. With increasing PANI content, the photocatalytic performance of PANI/TiO_2 gradually increased (Fig. 13(a)). When the content of PANI reached 4%, the photocatalytic efficiency of PANI/TiO_2 for degradation of phenol achieved its highest value (79.4%). When the ratio of PANI was beyond 4%, the photocatalytic performance decreased because the excess PANI absorbed part of the UV light. Conversely, the photocatalytic degradation efficiency of TiO_2 reached only 41.5%. Thus, it was obvious that the photocatalytic efficiencies of PANI/TiO_2 were higher than that of TiO_2 (P25), indicating that PANI promoted the electron-hole pairs separation [58].

More significantly, the photocatalytic performance of the ternary rGH-PANI/TiO_2 was obviously enhanced upon introduction of rGH (Fig. 13(b)). The degradation efficiency of 20%rGH-PANI/TiO_2 could reach 100% (the weight of rGH accounted for 20% of the total mass of rGH-PANI/TiO_2, the weight of PANI occupied 4% of the total mass of PANI/TiO_2). This was much higher than that of X rGH-PANI/TiO_2 (X = 10%, 30%, 50%, and 80%). The excessive rGH might have absorbed more UV light and competed with PANI/TiO_2 at absorbing light [59]. In addition, the adsorption capacity of TiO_2 for phenol was weak (Fig. 13(b)). Naturally, rGH-PANI/TiO_2 could adsorb only a small amount of phenol, and this should be attributed to π-π stacking and hydrogen bonding interactions between phenol and grapheme [60]. Therefore, a series of experiments conducted in the following study was based on 20% rGH-PANI/TiO_2.

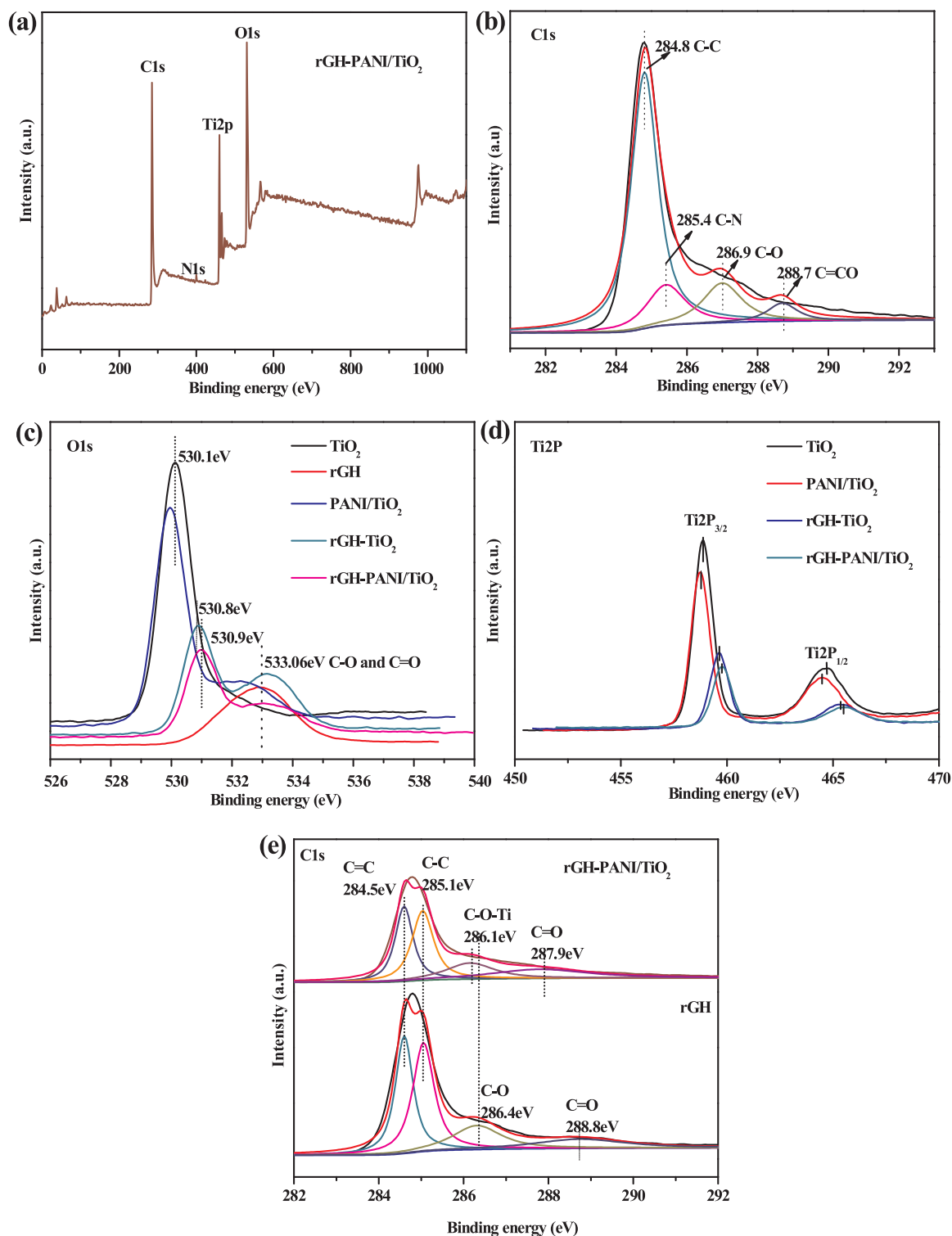The working potential has a crucial influence on the PEC

Fig. 7. (a) XPS survey spectra of rGH-PANI/TiO$_2$; (b) C1s spectra of rGH-PANI/TiO$_2$; (c) O1s spectra of different samples; (d) Ti2P spectra of different samples; and (e) C1s spectra of rGH-PANI/TiO$_2$ and rGH.

degradation of phenol. Thus, the potential should be optimized before the experiment. The PEC efficiency significantly increased when the potential was 0.5 to 1.0 V (Fig. 14(a)). The maximal efficiency for degradation of phenol was at 1.0 V. The enhanced degradation efficiency mainly was due to the space charge layer that grew wider as the potential increased [61]. However, the PEC performance of rGH-PANI/ TiO$_2$ gradually decreased when the applied potential was beyond 1.0 V, which should be due to the reallocation of the space charge layer and

the Hector Helmholtz layer [62]. Meanwhile, the polymer generated from phenol gathering on the rGH-PANI/TiO$_2$ possibly decreased degradation performance [61]. The efficiencies of rGH-PANI/TiO$_2$ for PEC degradation of phenol at various potentials are shown in Fig. 14(b).

Fig. 15 shows the efficiencies of rGH-PANI/TiO$_2$ for PEC degradation of various initial concentrations of phenol. The efficiencies of the ternary system for degradation of 5 mg/L and 20 mg/L phenol were 78.7% and 89%, respectively. However, the efficiency of rGH-PANI/
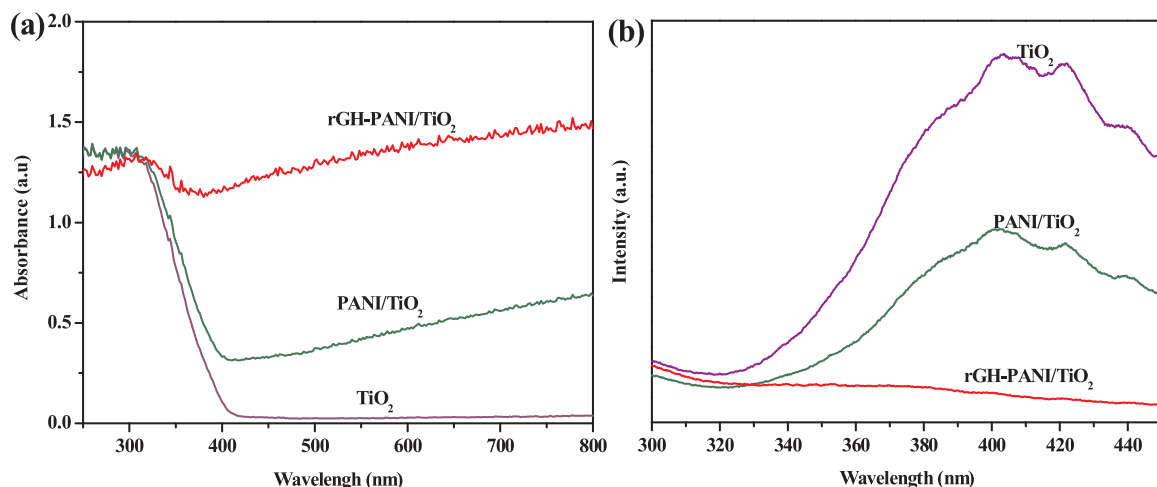
Fig. 8. (a) UV–vis diffuse reflectance spectra of different samples, (b) photoluminescence spectra of the different samples.
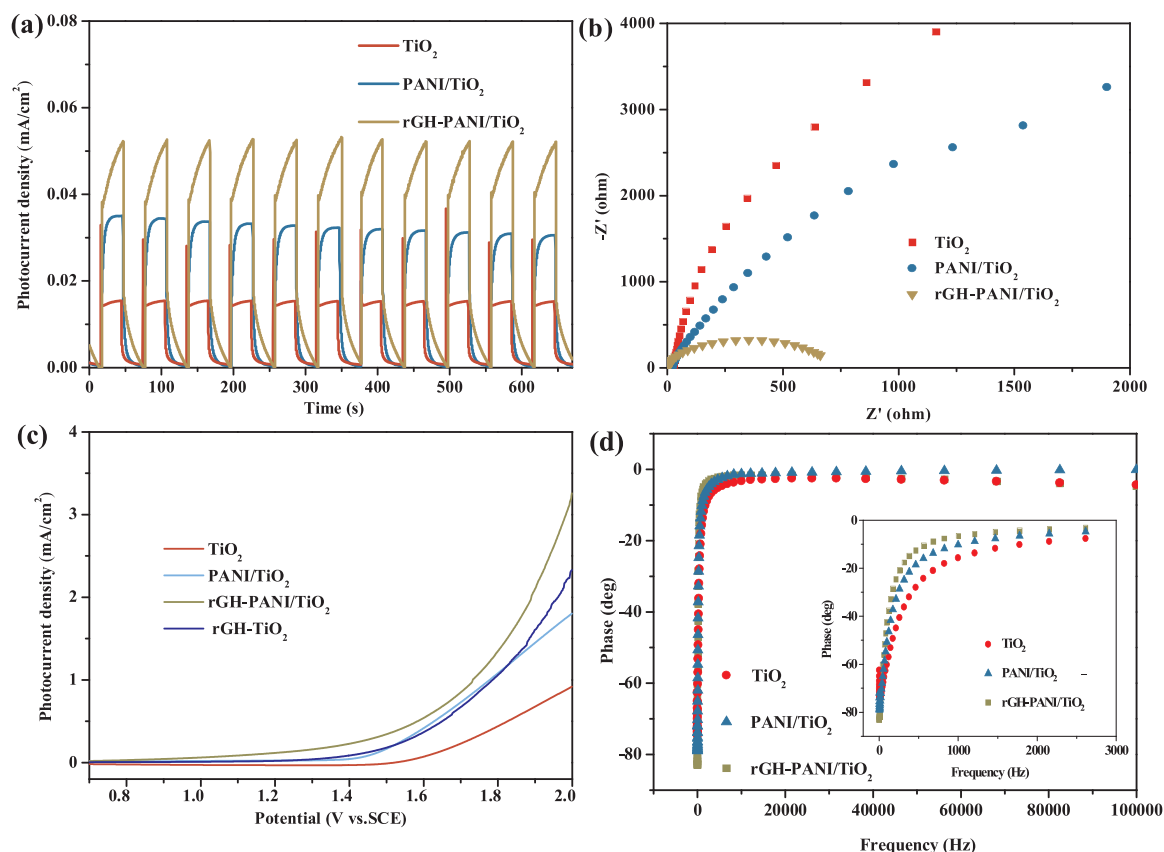

Fig. 9. (a) Transient photocurrent responses of photoelectrodes; (1.0 V bias, 500 W mercury lamp, $\lambda \geq 320$ nm); (b) EIS plots of photoelectrodes, (c) variation of photocurrent density vs. applied potential of photoelectrodes; and (d) Bode phase plots of the photoelectrodes.

TiO$_2$ for degradation of phenol 10 mg/L was 100%. When the phenol concentration was low, and the initial concentration of organic contaminants increased, then the number of phenol molecules adsorbed on the surface of rGH gradually increased, and the contact probability between organic molecules and $\cdot O_2^-$ increased, which leaded to the increasing of the degradation efficiency. In contrast, the degradation efficiency began to decrease if the phenol concentration exceeded a certain concentration. This might be due to the fact the active sites were occupied by phenol. This decreased the number of $\cdot O_2^-$ with a higher phenol concentration [63]. Therefore, 10 mg/L phenol was used for further studies.

Similar to the conventional electrochemical process, the concentrations of electrolyte can affect the PEC process. As shown in Fig. 16, different Na$_2$SO$_4$ solutions were selected as the electrolyte to study the effect of concentrations on the PEC degradation of phenol (Fig. 16). When the Na$_2$SO$_4$ concentration was lower than 100 mmol/L, the degradation efficiencies decreased with increasing Na$_2$SO$_4$ concentrations. This might be ascribed to the fact that the active sites of the catalyst surface were occupied by more ions with increasing Na$_2$SO$_4$ concentrations, reducing the contact sites between the contaminants and the catalysts [64].

In contrast, the degradation efficiency increased with increasing Na$_2$SO$_4$ concentrations when the Na$_2$SO$_4$ concentration exceeded 100 mmol/L. This was mainly due to the Na$_2$SO$_4$ in the solution
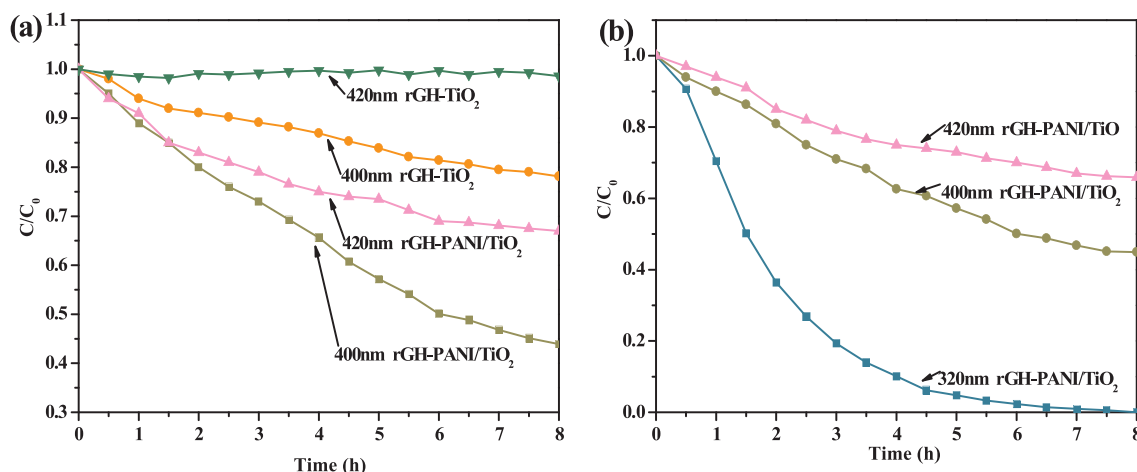
Fig. 10. (a) PEC degradation of phenol by rGH-TiO$_2$ and rGH-PANI/TiO$_2$ at different wavelengths; and (b) PEC degradation of phenol by rGH-PANI/TiO$_2$ at different wavelengths (the concentration of phenol is 10 mg/L, 1.0 V bias, and 500 W mercury lamp).
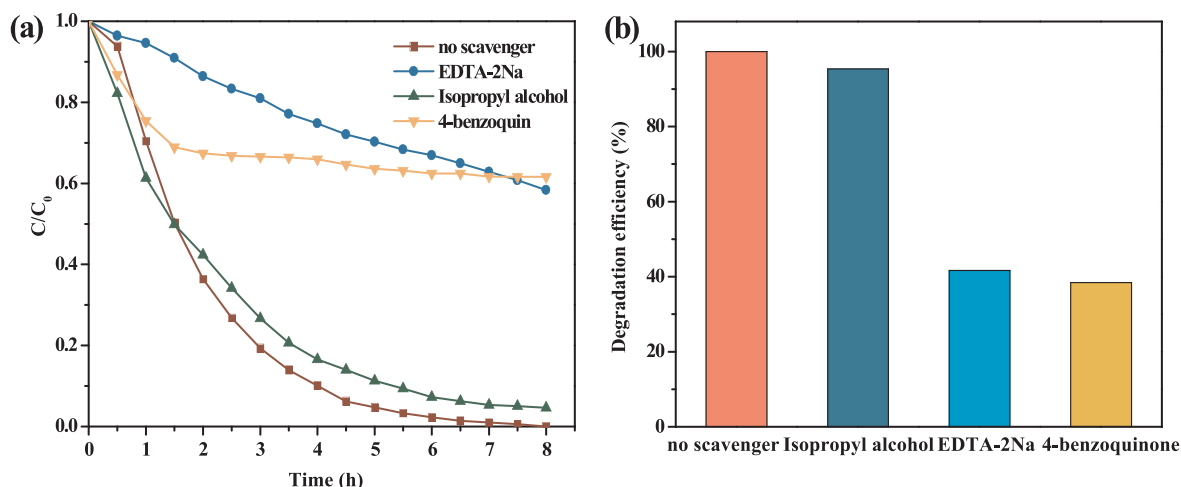

Fig. 11. (a) Plots of photo-generated active species trapped in the system of degradation of phenol by rGH-PANI/TiO$_2$ (the concentration of phenol was 10 mg/L, 1.0 V bias, 500 W mercury lamp, λ ≥ 320 nm); and (b) active species trapped in the system of degradation efficiency of phenol by rGH-PANI/TiO$_2$.
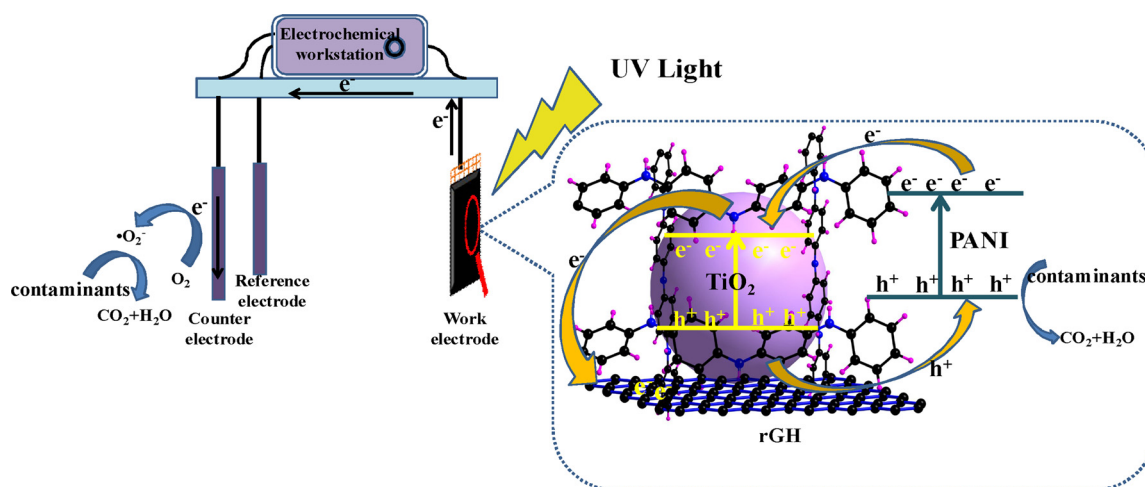

Fig. 12. PEC degradation mechanism of rGH-PANI/TiO$_2$ composite under UV light.

produced a charge-shielding effect that shielded the electrostatic repulsion between the adsorbed phenol and was not adsorbed on the surface of the rGH. This increased the adsorption capacity of rGH. In addition, a large amount of Na$_2$SO$_4$ in the solution would have a salting-out effect and reduced the solubility of phenol in solution; thus,

more phenol molecules were adsorbed on the active sites and facilitated the catalytic degradation of phenol.

Fig. 17 shows the influence of different pH on the activity of rGH-PANI/TiO$_2$ for PEC degradation of phenol (10 mg/L). The degradation efficiency of phenol in acidic and neutral solution reached more than
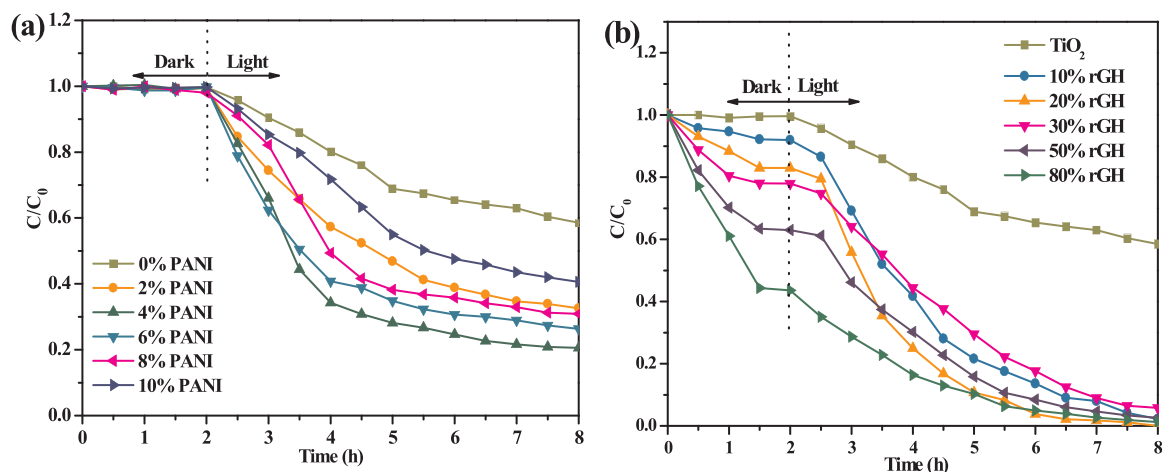
Fig. 13. (a) Photocatalytic degradation of phenol over PANI/TiO$_2$ at different weight ratios of PANI; (b) Photocatalytic degradation of phenol over rGH-PANI/TiO$_2$ at different weight ratios of rGH (the concentration of phenol was 10 mg/L, 500 W mercury lamp, λ ≥ 320 nm).
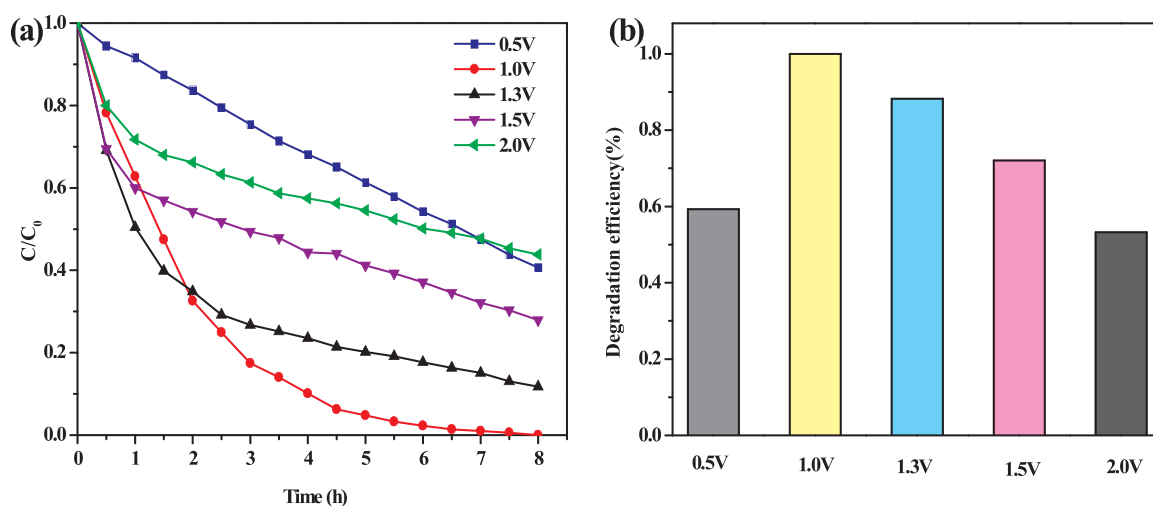

Fig. 14. (a) Comparison of the PEC degradation of phenol over rGH-PANI/TiO$_2$ photoelectrode at various potentials; and (b) PEC degradation efficiency of phenol over rGH-PANI/TiO$_2$ photoelectrode at various potentials.
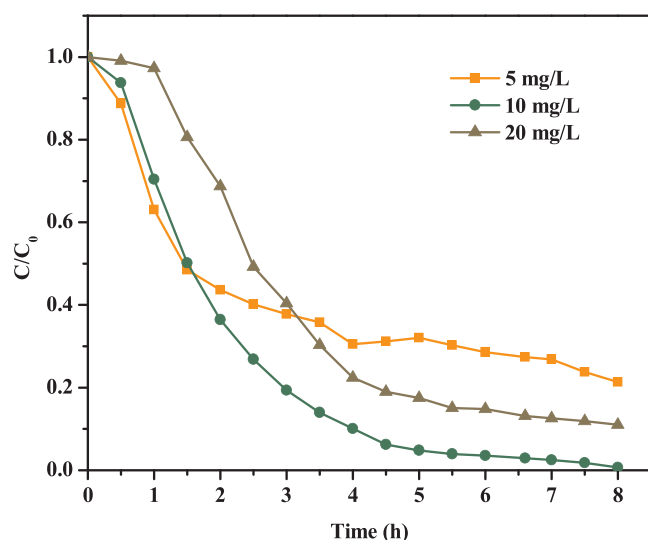

Fig. 15. rGH-PANI/TiO$_2$ PEC degradation of phenol with different initial concentrations (1.0 V bias, 500 W mercury lamp, λ ≥ 320 nm).
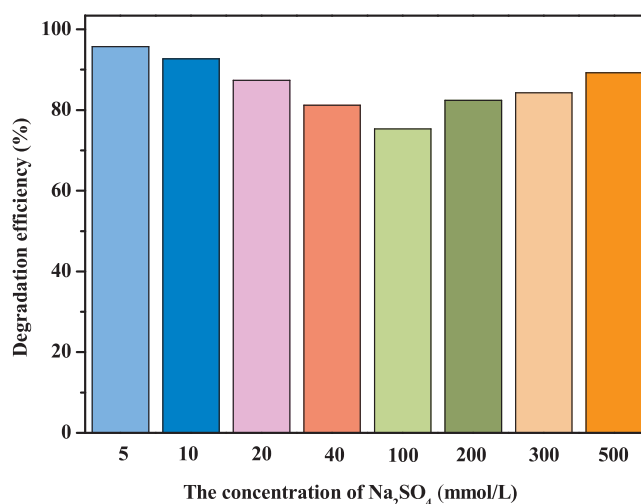
Fig. 16. Different Na$_2$SO$_4$ concentrations affect the PEC degradation of phenol at rGH-PANI/TiO$_2$ (the concentration of phenol is 10 mg/L, 1.0 V bias, 500 W mercury lamp, λ ≥ 320 nm).
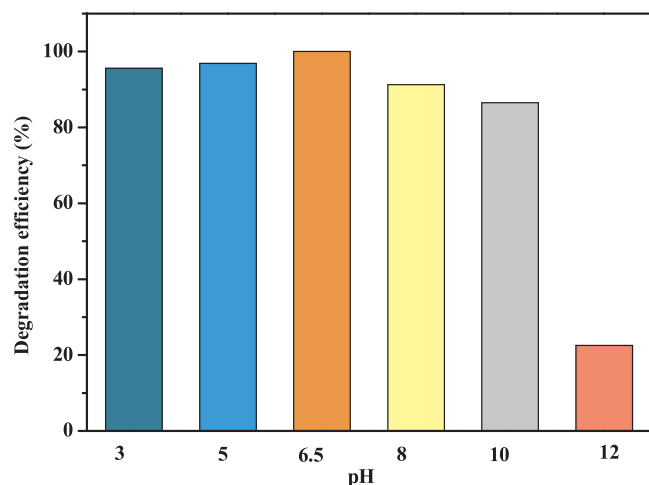
Fig. 17. PEC degradation of phenol by rGH-PANI/TiO$_2$ photoelectrode with different phenol solution pH values: (1.0 V bias, 500 W mercury lamp, $\lambda \geq 320$ nm).
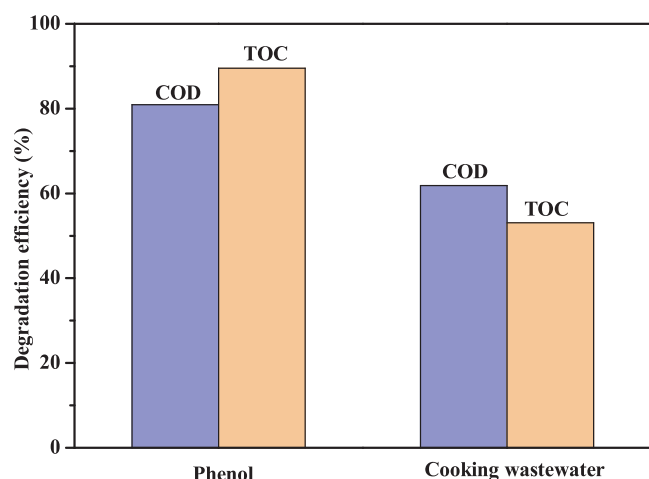

Fig. 18. The removal rates of TOC and COD in the PEC degradation process of phenol and coking wastewater by rGH-PANI/TiO$_2$ photoelectrode, (1.0 V bias, 500 W mercury lamp, $\lambda \geq 320$ nm).
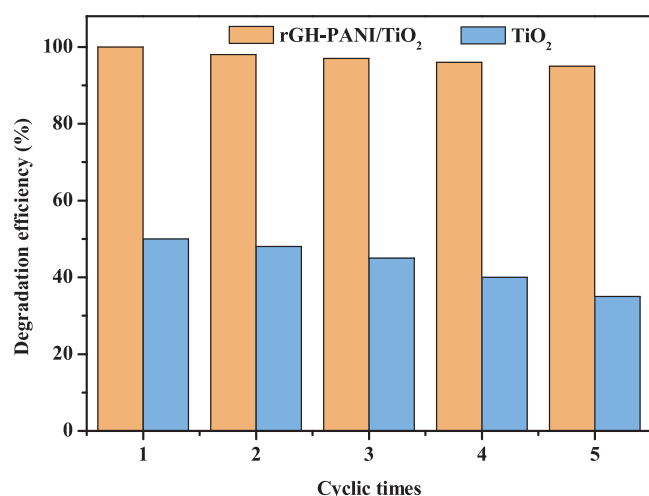

Fig. 19. Recycling performance for phenol degradation within five cycles for rGH-PANI/TiO$_2$ photoelectrodes. (The concentrations of phenol were 10 mg/L, 1.0 V bias, 500 W mercury lamp, $\lambda \geq 320$ nm.).

95% (Fig. 17), which should be due to most of the phenol molecules were adsorbed on the photoelectrode surface for rapid *in situ*

degradation. The degradation efficiency of phenol in alkaline solutions obviously decreased the degradation efficiency was only 22.5% at pH 12. This was mainly because the surface of PANI/TiO$_2$ was negatively charged in the alkaline solution; the phenol intermediate was dissociated with negative charges. Because of electrostatic repulsion, the phenol intermediate was poorly adsorbed on the surface of the catalyst. This reduced the degradation efficiency of phenol [36]. The PEC degradation efficiencies reached more than 80% when pH varied from 2 to 10, indicating that the rGH-PANI/TiO$_2$ photoelectrode maintained a high catalytic performance across a wide pH range (Fig. 17).

To evaluate the efficiency of rGH-PANI/TiO$_2$ for mineralizing coking wastewater and phenol, the TOC and COD removal rates were examined in the PEC degradation processes under UV light irradiation at a bias voltage of 1.0 V with a 320 nm cut-off filter. Coking wastewater was selected as a practical contaminant. The initial COD values for coking wastewater and phenol (10 mg/L) were 60 mg/L and 9.9 mg/L, respectively. As shown in Fig. 18, the TOC and COD removal rates of phenol were 89.5% and 80.9%, respectively, which indicated that the surface of the composite photocatalyst enhanced the mineralization efficiency of contaminants. Therefore, rGH-PANI/TiO$_2$ demonstrated advantages in PEC degradation of coking wastewater and other refractory organic compounds.

The stability of rGH-PANI/TiO$_2$ photoelectrode was also evaluated by five cycling degradation experiments (Fig. 19). Each degradation experiment lasted 8 h. After each cycle, the working electrode was washed three times with deionized water, then continuing to be used for the next cycle. The degradation efficiency of the ternary composite remained above 95% with only 5.0% decreasing after five cycles; the degradation efficiency of TiO$_2$ film decreased by 15%. These results revealed that the prepared rGH-PANI/TiO$_2$ photoelectrodes exhibited high stability and PEC performance. This high degradation performance was mainly attributed to the introduction of PANI and rGH, which formed the C–Ti bonds and hydrogen bonds [43,65]. In addition, the large π bond on rGH also facilitated the rapid electron transfer to the metal titanium mesh. This separated the electron-hole pairs. The TiO$_2$ nanoparticles are distributed evenly on the surface of Graphene with which the porous 3D structure of Graphene hydrogel constructed and showing more catalytic active sites. Thus the efficiency of rGH-PANI/TiO$_2$ photoelectrodes can be maintained above 95% after five cycling degradation experiments.

4. Conclusion

In summary, the prepared ternary rGH-PANI/TiO$_2$ composite hydrogels with a 3D network structure have a highly efficient photocatalyst via a surface hybridization and water bath method. The ternary composite exhibited a high PEC performance for the degradation of phenols and coking wastewater. The PEC degradation efficiencies of rGH-PANI/TiO$_2$ for the degradation of phenol, 2,4-dichlorophenol, and BPA could reach 100% after 7 h, 3.5 h, and 4.5 h, respectively. In addition, 53.1% of the TOC and 71.9% of the COD in coking wastewater was removed in 8 h of UV light irradiation with a 320 nm cut-off filter. The high PEC activity and mineralization efficiency of rGH-PANI/TiO$_2$ composite were attributed to the hybridization of PANI and rapid transfer of electrons for rGH. Meanwhile, the rGH-PANI/TiO$_2$ hydrogel formed a 3D network structure with a large specific surface area that provided more active sites for the *in situ* PEC degradation of organic pollutants. More catalysts also could be immobilized on the hydrogels and could solve the problem whereby it is difficult to remove powder catalysts and they are prone to produce secondary pollution. In summary, the results show that an rGH-PANI/TiO$_2$ photoelectrode with a 3D network structure has good degradation and mineralization ability for many organic contaminants. In addition, the synergistic effects between photocatalysis and electrocatalysis significantly improved the degradation and mineralization efficiency of phenolic compounds, making the PEC process an effective tool for wastewater remediation.

Acknowledgments

References

[1] Y. Zhang, Q. Wang, J. Lu, Q. Wang, Y. Cong, Chemom. Intell. Lab. Syst. 162 (2016) 55–63.
[2] P. Yilmaz, A.M. Lacerda, I. Larrosa, S. Dunn, Electrochim. Acta 231 (2017) 641–649.
[3] A.B. Laursen, S. Kegnaes, S. Dahl, I. Chorkendorff, Energy Environ. Sci. 5 (2012) 5577–5591.
[4] Y. Wei, J. Su, X. Wan, L. Guo, L. Vayssieres, Nano Res. 9 (2016) 1561–1569.
[5] E. Kalamaras, V. Dracopoulos, L. Sygellou, P. Lianos, Chem. Eng. J. 295 (2016) 288–294.
[6] H. Zeng, S. Liu, B. Chai, D. Cao, Y. Wang, X. Zhao, Environ. Sci. Technol. 50 (2016) 6459–6466.
[7] X. Zhao, J. Zhang, M. Qiao, H. Liu, J. Qu, Environ. Sci. Technol. 49 (2015) 4567–4574.
[8] X. Chen, Q. Chen, W. Jiang, Z. Wei, Y. Zhu, Appl. Catal. B 211 (2017) 106–113.
[9] R. Chen, X. Cheng, X. Zhu, Q. Liao, L. An, D. Ye, X. He, Z. Wang, Chem. Eng. J. 316 (2017) 911–918.
[10] G. Yang, D. Chen, H. Ding, J. Feng, J. Zhang, Y. Zhu, S. Hamid, D.W. Bahnemann, Appl. Catal. B 219 (2017) 611–618.
[11] F. Tavella, C. Ampelli, L. Frusteri, F. Frusteri, S. Perathoner, G. Centi, Catal. Today 304 (2017) 190–198.
[12] L. Jia, X. Sun, Y. Jiang, S. Yu, C. Wang, Adv. Funct. Mater. 25 (2015) 1814–1820.
[13] Y.M. Hunge, M.A. Mahadik, A.V. Moholkar, C.H. Bhosale, Appl. Surf. Sci. 420 (2017) 764–772.
[14] C. Terashima, R. Hishinuma, N. Roy, Y. Sugiyama, S.S. Latthe, K. Nakata, T. Kondo, M. Yuasa, A. Fujishima, Appl. Mater. Interfaces 8 (2016) 1583–1588.
[15] J. Quiñonero, T.L. Villarreal, R. Gómez, Appl. Catal. B 194 (2016) 141–149.
[16] Z. Wei, F. Liang, Y. Liu, W. Luo, J. Wang, W. Yao, Y. Zhu, Appl. Catal. B 201 (2017) 600–606.
[17] D. Wang, X. Li, J. Chen, X. Tao, Chem. Eng. J. 198-199 (2012) 547–554.
[18] M. Adachi, Y. Murata, J. Takao, J. Jiu, M. Sakamoto, F. Wang, J. Am. Chem. Soc. 126 (2004) 14943–14949.
[19] D. Dinda, A. Gupta, S.K. Saha, J. Mater. Chem. A 1 (2013) 11221–11228.
[20] C. Li, G. Shi, Nanoscale 4 (2012) 5549–5563.
[21] J. Yang, D. Chen, Y. Zhu, Y. Zhang, Y. Zhu, Appl. Catal. B 205 (2017) 228–237.
[22] A.K. Geim, K.S. Novoselov, Nat. Mater. 6 (2007) 183.
[23] S. Stankovich, D.A. Dikin, G.H.B. Dommett, K.M. Kohlhaas, E.J. Zimney, E.A. Stach, R.D. Piner, S.T. Nguyen, R.S. Ruoff, Nature 442 (2006) 282.
[24] Y. Zhang, W. Cui, W. An, L. Liu, Y. Liang, Y. Zhu, Appl. Catal. B 221 (2018) 36–46.
[25] Y. Li, W. Cui, L. Liu, R. Zong, W. Yao, Y. Liang, Y. Zhu, Appl. Catal. B 199 (2016) 412–423.
[26] G. Yang, W. Hou, X. Feng, L. Xu, Y. Liu, G. Wang, W. Ding, Adv. Funct. Mater. 17 (2007) 401–412.
[27] J. Hou, R. Cao, S. Jiao, H. Zhu, R.V. Kumar, Appl. Catal. B 104 (2011) 399–406.
[28] K. Pandiselvi, H. Fang, X. Huang, J. Wang, X. Xu, T. Li, J. Hazard. Mater. 314 (2016) 67–77.
[29] G.M. Neelgund, V.N. Bliznyuk, A. Oki, Appl. Catal. B 187 (2016) 357–366.
[30] L. Jing, Z. Yang, Y. Zhao, Y. Zhang, X. Guo, Y. Yan, K. Sun, J. Mater. Chem. 2 (2014) 1068–1075.
[31] W. Jiang, W. Luo, R. Zong, W. Yao, Z. Li, Y. Zhu, Small 12 (2016) 4370–4378.
[32] H. Wang, C. Guan, X. Wang, H.J. Fan, Small 11 (2015) 1470–1477.
[33] Y. Xu, K. Sheng, C. Li, G. Shi, ACS Nano 4 (2010) 4324–4330.
[34] Y. Duan, Q. Tang, Z. Chen, B. He, H. Chen, J. Mater. Chem. 2 (2014) 12459–12465.
[35] J. Luo, S. Jiang, Y. Wu, M. Chen, X. Liu, J. Polym. Sci. 50 (2012) 4888–4894.
[36] H. Wang, Y. Liang, L. Liu, J. Hu, P. Wu, W. Cui, Appl. Catal. B 208 (2017) 22–34.
[37] X. Tao, X. Chen, Y. Xia, H. Huang, Y. Gan, R. Wu, F. Chen, W. zhang, J. Mater. Chem. 1 (2013) 3295–3301.
[38] S. Chatterjee, R.K. Layek, A.K. Nandi, Carbohydr. Res. 52 (2013) 509–519.
[39] W. Zhang, H. Guo, H. Sun, R. Zeng, Appl. Surf. Sci. 410 (2017) 547–556.
[40] S. Bera, H. Khan, I. Biswas, S. Jana, Appl. Surf. Sci. 383 (2016) 165–176.
[41] H. Zhang, R. Zong, Y. Zhu, J. Phys. Chem. 113 (2009) 4605–4611.
[42] Z. Li, H. Zhang, Q. Liu, Y. Liu, L. Stanciu, J. Xie, Carbohydr. Res. 71 (2014) 257–267.
[43] S.D. Perera, R.G. Mariano, K. Vu, N. Nour, O. Seitz, Y. Chabal, K.J. Balkus, ACS Catal. 2 (2012) 949–956.
[44] C. Zhen, T. Wu, M.W. Kadi, I. Ismail, G. Liu, H. Cheng, Chin. J. Catal. 36 (2015) 2171–2177.
[45] Y. Deng, L. Tang, G. Zeng, H. Dong, M. Yan, J. Wang, W. Hu, J. Wang, Y. Zhou, J. Tang, Appl. Surf. Sci. 387 (2016) 882–893.
[46] W. Zhang, X. Xiao, Y. Li, X. Zeng, L. Zheng, C. Wan, Appl. Surf. Sci. 389 (2016) 496–506.
[47] X. Bai, L. Wang, Y. Wang, W. Yao, Y. Zhu, Appl. Catal. B 152–153 (2014) 262–270.
[48] X. Gao, W. Sun, Z. Hu, G. Ai, Y. Zhang, S. Feng, F. Li, L. Peng, J. Phys. Chem. C 113 (2009) 20481–20485.
[49] A.G. Tamirat, W. Su, A.A. Dubale, C.-J. Pan, H. Chen, D.W. Ayele, J.F. Lee, B.J. Hwang, J. Power Sources 287 (2015) 119–128.
[50] Y. Lin, D. Li, J. Hu, G. Xiao, J. Wang, W. Li, X. Fu, J. Phys. Chem. C 116 (2012) 5764–5772.
[51] L. Liu, L. Ding, Y. Liu, W. An, S. Lin, Y. Liang, W. Cui, Appl. Catal. B 201 (2017) 92–104.
[52] J. Guo, Y. Liu, Y. Hao, Y. Li, X. Wang, R. Liu, F. Li, Appl. Catal. B 224 (2018) 841–853.
[53] S. Liu, F. Li, Y. Li, Y. Hao, X. Wang, B. Li, R. Liu, Appl. Catal. B 212 (2017) 115–128.
[54] D. Chen, K. Wang, D. Xiang, R. Zong, W. Yao, Y. Zhu, Appl. Catal. B 147 (2014) 554–561.
[55] S. Tan, J. Zhai, B. Xue, M. Wan, Q. Meng, Y. Li, L. Jiang, D. Zhu, Langmuir 20 (2004) 2934–2937.
[56] Y. Hao, B. Liu, L. Tian, F. Li, J. Ren, S. Liu, Y. Liu, J. Zhao, X. Wang, A.C.S. Appl, Mater. Inter. 9 (2017) 12687–12693.
[57] A. Santos, P. Yustos, T. Cordero, S. Gomis, S. Rodríguez, F. García-Ochoa, Catal. Today 102-103 (2005) 213–218.
[58] H. Zhang, R. Zong, J. Zhao, Y. Zhu, Environ. Sci. Technol. 42 (2008) 3803–3807.
[59] X. Liu, L. Pan, Q. Zhao, T. Lv, G. Zhu, T. Chen, T. Lu, Z. Sun, C. Sun, Chem. Eng. J. 183 (2012) 238–243.
[60] X. Wang, S. Huang, L. Zhu, X. Tian, S. Li, H. Tang, Carbohydr. Res. 69 (2014) 101–112.
[61] Z. Wei, F. Liang, Y. Liu, W. Luo, J. Wang, W. Yao, Y. Zhu, Appl. Catal. B 201 (2017) 600–606.
[62] Z. Li, W. Luo, M. Zhang, J. Feng, Z. Zou, Energy Environ. Sci. 6 (2013) 347–370.
[63] I.K. Konstantinou, T.A. Albanis, Appl. Catal. B 49 (2004) 1–14.
[64] J. Xu, L. Wang, Y. Zhu, Langmuir 28 (2012) 8418–8425.
[65] M. Wei, J. Wan, Z. Hu, Z. Peng, B. Wang, Appl. Surf. Sci. 377 (2016) 149–158.